Global Journal of Science Frontier Research
Volume 11 Issue 1 Version 1.0 February 2011
Type: Double Blind Peer Reviewed International Research Journal
Publisher: Global Journals Inc. (USA)
ISSN: 0975-4350

Phonon Dispersion and Specific Heat Calculation of Poly 3,3-Dimethyloxetane

By Ajita Pathak,Geetika Srivastava,Piyush Tripathi
Amity University(Department of Amity school of engineering and technology)

Abstracts Vibrational dynamics of the poly 3,3-dimethyloxetane (form III) is being reported using Higg's method and Urey Bradley force field. Characteristic features of dispersion curves such as repulsion, crossing and bunching are reported. A comparitive study of the two polymorphic forms (form II and III) is presented and possible regions for variation in heat capacity are discussed.

Keywords: 3,3-dimethyloxetane,repulsion,bunching, dispersion profiles,density-of- states, heat capacity.

Strictly as per the compliance and regulations of:

.

Phonon Dispersion and Specific Heat Calculation of Poly 3,3-Dimethyloxetane

Ajita Pathak[1],Geetika Srivastava[2],Piyush Tripathi[3]

Abstract- **Vibrational dynamics of the poly 3,3-dimethyloxetane (form III) is being reported using Higg's method and Urey Bradley force field. Characteristic features of dispersion curves such as repulsion, crossing and bunching are reported. A comparitive study of the two polymorphic forms (form II and III) is presented and possible regions for variation in heat capacity are discussed.**

Keywords:3,3-dimethyloxetane,repulsion,bunching, dispersion profiles,density-of- states, heat capacity.

I. Introduction

In several earlier publications [1-4], we have reported, studies on the vibrational dynamics of polymeric systems including synthetic polymers. In continuatation of this work, we report here phonon dispersion and specific heat variation in Poly (3,3dimethyloxetane).The branched polyether series generally have a variety of conformational forms, which lead to various crystalline structures. The structure, thermal behavior and crystallinity of these branched polyoxetanes have been studied by many authors [5-11]. Poly-oxetane structure is similar to that of polyether with general structure (-O-CH_2-CR_1R_2-CH_2-). Alkyl group R_1 and R_2 are responsible for variation in their properties. Poly (3, 3-dimethyloxetane) PDMO, exists in three different crystalline structure [9]. Form I is a planar zigzag conformation, form II T_3GT_3G has monoclinic structure and form III $(T_2G_2)_2$ is orthorhombic in structure. This orthorhombic unit cell has a =15.60A°, b = 5.74 A° and c = 6.51 A

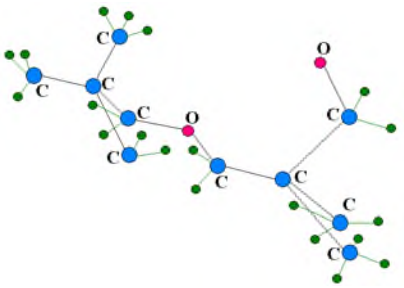

Figure 1. One complete unit of poly (3,3-dimethyloxetane)

About-Amity University(Department of Amity school of engineering and technology)Virajkhand 5, Gomtinagar Lucknow U.P. India
Email[1] -pathak_ajita@rediffmail.com
Email[2] -geetika_gkp@rediffmail.com
Email[3] - piyush.tripathi2007@gmail.com

From space group & molecular symmetry it appears that two molecular chains are located at the center & the corner of the unit cell so that the two fold screw axis and the two fold rotation axis of the molecule coincide with those of the space group. Raman and IR spectroscopic methods have been widely used in order to determine quantitatively the polymers microstructure. In some recent publications, synthesis and characterization of star-shaped poly (3, 3-dimethyloxetane) and mechanism of the polymerization process have studied by Youn pal et.al.[12]. The crystal structure of the two main crystalline forms of PDMO has been determined by Takahashi et.al. [5]. Vibrational analysis of poly (3, 3-dimethyloxetane) using valance force field reported by Meriono et al. [13]. Most of this work is limited either by the use of approximate force field, lack of dispersion curves and their eventual use in obtaining thermodynamic parameters. Such infirmities seriously effect not only assignments but also the profile of dispersion curves. Lack of information on dispersive behavior is responsible for incomplete understanding of polymeric spectra. In general, the infrared absorption, Raman spectra and inelastic neutron scattering from polymeric systems are very complex and cannot be unraveled without the full knowledge of dispersion curves. One cannot appreciate without it the origin of both symmetry dependent & symmetry independent spectral features. Further the presence of regions of high density-of-states, which appear in all these techniques and play an important role in thermo dynamical behavior, can be studied only from dispersion curves. It is therefore important to carry out a complete normal mode analysis.

In the present communication, a detailed comparative study of the two forms (modification II and modification III) of PDMO including dispersion curves is presented using Urey Bradley force field. Predictive values of heat capacity in range 10K to 300K are presented and comparative study of the two forms is made to identify the structure related spectral differences. These are found to be in good agreement with the experimental data to best of our knowledge. Lack of this information on dispersive behavior of normal modes in many polymeric systems has been responsible for incomplete understanding of polymer spectra. In general, the infrared absorption, Raman spectra and inelastic

infrared absorption, Raman spectra and inelastic neutron scattering from polymeric systems are very complex and cannot be unraveled without the full knowledge of dispersion curves. One cannot appreciate without it the origin of both symmetry dependent & symmetry independent spectral features. Further the presence of regions of high density-of-states, which appear in all these techniques and play an important role in thermo dynamical behavior, can be studied only from dispersion curves.

II. Calculation of normal mode frequencies

Normal mode calculation for a polymeric chain was carried out using Wilson's GF matrix [14] method as modified by Higgs [15] for an infinite polymeric chain. The vibrational secular equation to be solved is

$$|G(\delta)F(\delta)-\lambda(\delta)I| = 0 \qquad 0 \le \delta \le \pi$$

where δ is the phase difference between the modes of adjacent chemical units, G(δ) matrix is derived in terms of internal coordinates and inverse of it is kinetic energy and F(δ) matrix is based on Urey Bradley force field [16] which has certain advantages over other type of force field; such as valence force field, generalized force field.

1. Relatively less parameter are required to express the potential energy.
2. No quadratic cross terms are included in the potential energy expression. The interaction between non-bonded atoms includes these terms.
3. Arbitrariness in choosing the force constant is reduced.

The frequencies ν_i in cm^{-1} are related to eigen values by

$$\lambda_i(\delta) = 4\pi^2 c^2 \nu_i^2(\delta).$$

plot of $\nu_i(\delta)$ versus δ gives the dispersion curve for the th mode. The use of the type of force field is generally a matter of one's chemical experience and intuition. In the present work we have used Urey Bradley force field [16] that is more comprehensive then valence force field. Recently spectroscopically effective molecular mechanics model have been used for inter and intra molecular interactions consisting of charges, atomic dipoles and Vander Waals interactions [17].

III. Force constant evaluation

The force constants have been obtained by the least square fitting. In order to obtain the "best fit" with the observed frequencies, the following procedure is adopted. Initially, approximate force constants are transferred from PGA [3]. Thus starting with the approximate F matrix F_0 and the observed frequencies λ_{obs} (related through a constant). One can solve the secular matrix equation:

$$GF_0L_0 = L_0\lambda_0$$

Let $\Delta\lambda i = \lambda i_{obs} - \lambda i_0$ in the above equation. It can be shown that in the first order approximation

$$\Delta\lambda = j\Delta F$$

Where j is computed from L_0. We wish to compute the corrections to F_0 so that the errors $\overline{\Delta\lambda}$ are minimized. We use the theory of least square and calculate

$$j' p\overline{\Delta\lambda} = (j' pj)\overline{\Delta F} \qquad (1)$$

Where p is a weighting matrix and j' is the transpose of j. The solution to this equation is obtained by inverting $j' pj$ to give

$$\overline{\Delta F} = (j' pj)^{-1} j' p\overline{\Delta\lambda}$$

If the number of frequencies is greater than the number of F matrix elements, the matrix J'PJ should be nonsingular and we obtain the corrections ΔF, which will minimize the sum of the weighted squares of the residuals. If the corrections ΔF are fairly large, the linear relation between force constant and frequency term in the matrix Eq. (a) breaks down. In such a situation, further refinement using higher order terms in Taylor's series expansion of $\Delta\lambda_i$ is needed. This procedure is developed by King et al. [18].

IV. Calculation of specific heat

Dispersion curves can be used to calculate the specific heat of a polymeric system. For (3) one-dimensional system the density of state function or the frequency distribution function expresses the way energy is distributed among the various braches of normal modes in the crystal, is calculated from the relation

$$g(\nu) = \sum(\partial\nu_j/\partial\delta)^{-1}]_{\nu j(\delta)=\nu j}$$

The sum is over all the branches j. Considering a solid as an assembly of harmonic oscillators, the frequency distribution g (ν) is equivalent to a partition function. The constant volume heat capacity can be calculated using Debye's relation

$$C_v = \sum g(\nu_j) K N_A (h\nu_j/KT)^2 [\exp(h\nu_j/KT)/\{\exp(h\nu_j/KT)-1)\}^2]$$

$$\text{with} \quad g(\nu_i)\, d\nu_i = 1$$

V. Results and Discussion

In a PDMO there are 16 atoms per residue unit giving rise to 48 dispersion curves and 44 optically active modes. The Cartesian coordinates were obtained by molecular modeling and energy minimization techniques which are consistent with the structure reported by Takahashi et al. [5]. The vibrational frequencies are calculated for δ values ranging from 0 to π in steps of $.05\pi$. A chemical repeat unit of PDMO is shown in Fig. [5.1]. Initially, force constants were transferred from planar PGA [3], and other similar polymer and then modified to obtain the "best fit" to the observed infrared (FT-IR) [13], Fig. [5.2] and Raman spectra [13], Fig. [5.3]. The Infra red spectra of PDMO II is shown in fig. [5.4].The final force constants along with the internal coordinate are given in Table [5.1]. The force constants given in parenthesis are due to non-bonded interactions. Since the modes above 1300 cm^{-1} are almost non-dispersive in nature, dispersion curves are plotted in Figs. 2(a) & 3(a) for the modes below 1300 cm^{-1}. The frequencies along with their PED are given in Table [5.2] and Table [5.3].The lowest four modes at $(\omega=0)$, $(\delta=0)$ and $(\omega=0)$, $(\delta=\pi)$ are called acoustic modes. The agreement between observed and the calculated frequencies is good. The assignments have been made on the basis of potential energy distribution (PED), band shape, band intensity and appearance/disappearance of modes in similar molecules with atoms placed in similar environment. For the sake of simplicity, modes are discussed under two heads; non-dispersive and dispersive.

VI. Non-Dispersive Modes

The non dispersive modes are highly localized in nature. The free stretching modes generally behave in this manner; e.g. C-H stretch.CH_3 asymmetric and symmetric stretches appear in region 2968 cm^{-1} and 2870 cm^{-1}. These values are same which are observed in Raman spectra. Similarly, CH_2 asymmetric and symmetric stretches are non-dispersive in nature and there frequencies are shown in Table [5.2]The deformation vibration of δ (CH_3) gives rise to absorption in the region 1400 cm^{-1}-1500 cm^{-1}. This mode is calculated at 1485 cm^{-1} and the corresponding peak is observed at 1485 cm^{-1} in Raman spectra. CH_2 deformation mode is calculated at 1475 cm^{-1} and 1452 cm^{-1} and the corresponding peaks are at the same value in Raman spectra. These two frequencies correspond to the two CH_2 groups present in the repeat unit. A comparison of modes of PDMO modification II with PDMO modification III is shown in Table (5.4) which indicates that most of the non-dispersive modes are well localized and are not much affected by the conformational changes.

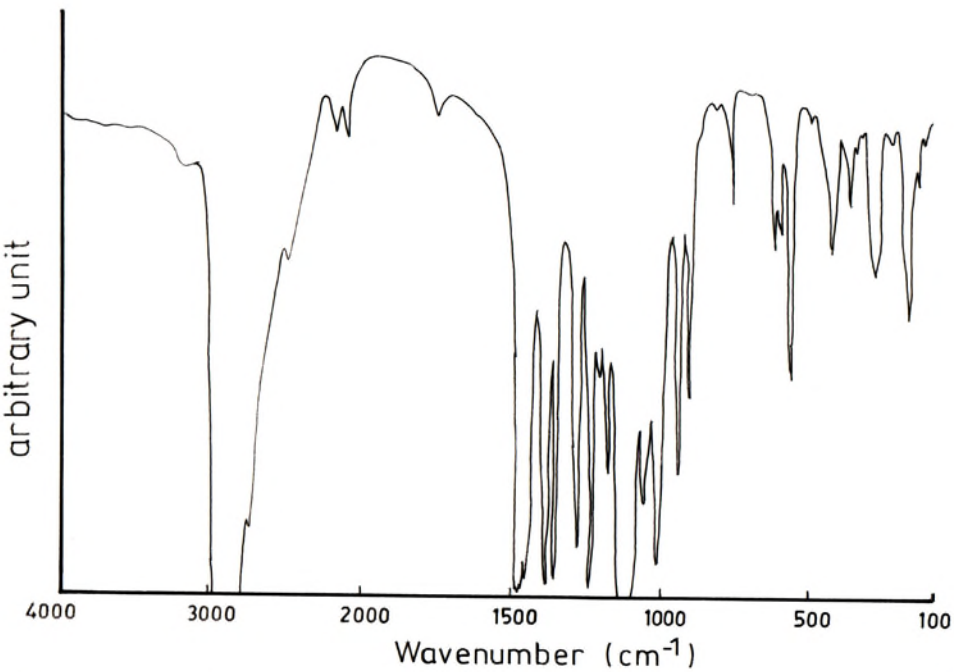

Figure5.2- Infra-red spectrum of PDMO in conformation III .

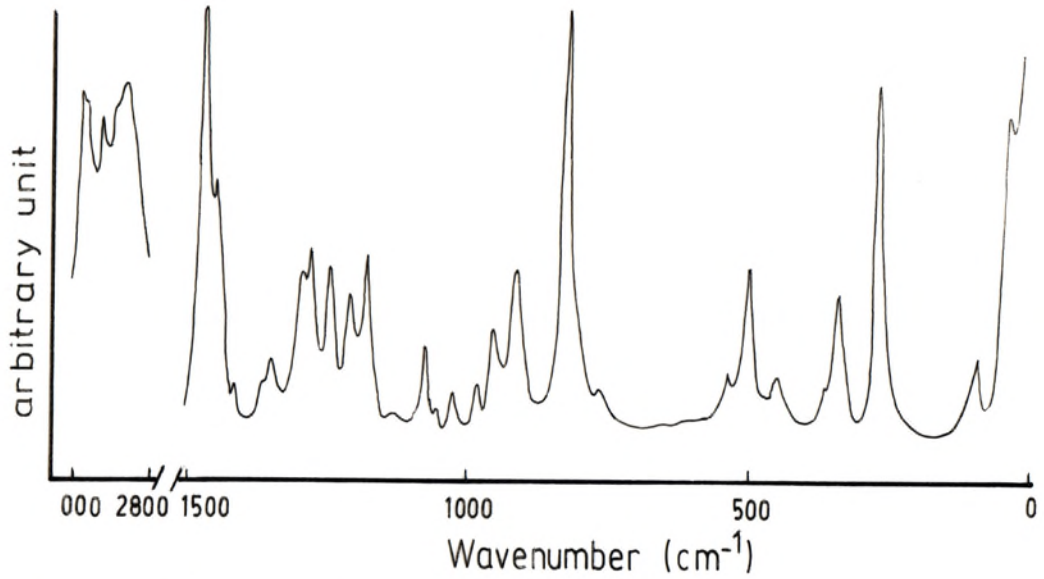

Figure5.3-Raman spectrum of PDMO in conformation III.

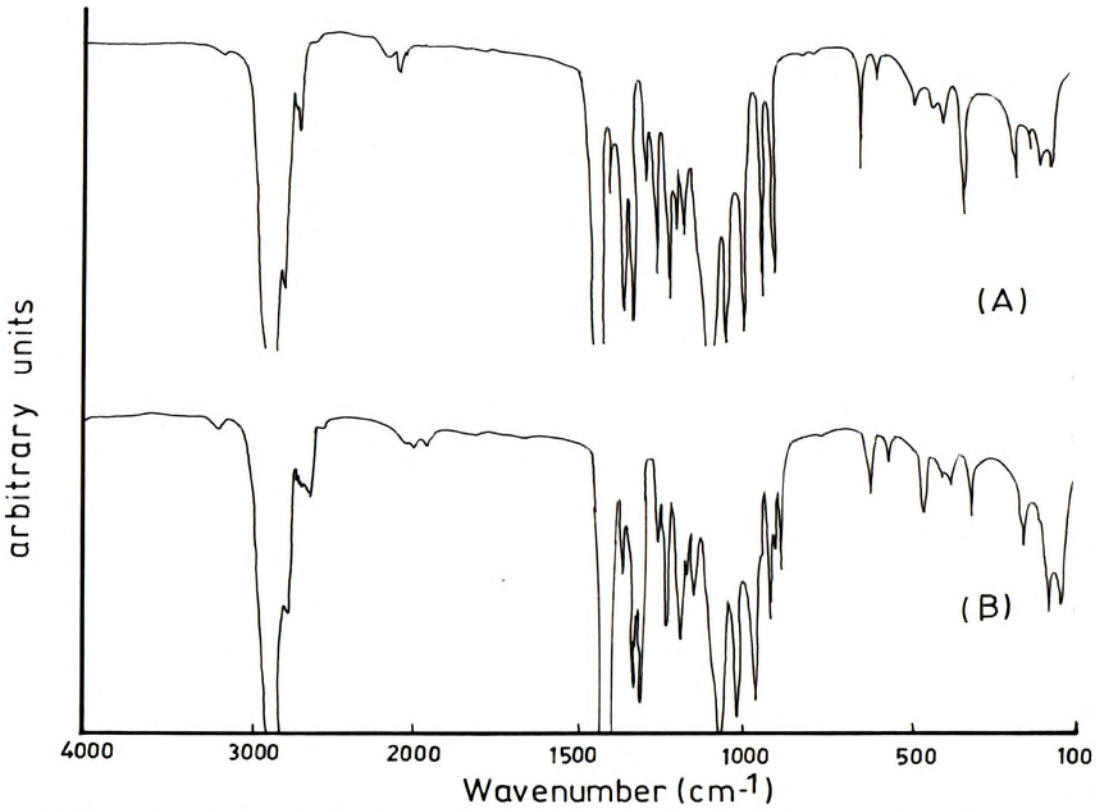

Figure5.4-Polarized infra-red PDMO in conformation II.

(A) Perpendicular

(B)Parallel

VII. Dispersive modes

The modes, which are dispersive, are mixed modes that are highly coupled along the chain. Their assignments are given in table 3. CH_2 rocking and C-O stretching appear in the region 1000 cm^{-1} to 1050 cm^{-1}, showing their peaks at 1006 cm^{-1} and 1017 cm^{-1} respectively at zone center. These values correspond to the peaks at 1006 cm^{-1} in Raman spectra and at 1017 cm^{-1} in I.R spectra respectively. The region between (1000-800) cm^{-1} is dedicated to conformational sensitive modes. These modes are characteristic modes of asymmetric and symmetric (C-O) stretch mixed with CH_3 rocking. The observed peaks in this region are well assigned by calculated frequencies. C-O asymmetric stretch appears at 955 cm^{-1} at the zone boundary and observed peak in Raman spectra is at 948 cm^{-1}. Peak at 909 cm^{-1} is a mixed mode of CH_3 twist with C-C stretching. This mode is calculated at 910 cm^{-1}, which agrees well with the observed value. Observed value of 873 cm^{-1}mode is calculated at 893 cm^{-1} at the zone centre and at 883 cm^{-1} at the zone boundary, which is the mixed mode of CH_2 rocking and (C-O-C) inplane bending. The most important result, which distinct two conformations of this compound is due to band intensity at 804 cm^{-1} (form II) and 822 cm^{-1} (form III) in Raman spectra [13]. This mode is one of the characteristic features of PDMO form III and is calculated at 816 cm^{-1} at the zone centre. This results from the contribution of motion of the side groups. These characteristic bands of PDMO are a good key to identifying the conformational variations. Modes below 800 cm^{-1} calculated at 575 cm^{-1}, 507 cm^{-1}, 449 cm^{-1}, 385 cm^{-1} and 355 cm^{-1} are all skeletal modes and are in good agreement with the observed modes at 575 cm^{-1}, 490 cm^{-1}, 442 cm^{-1},385 cm^{-1}, and 354 cm^{-1} respectively, which arise from the skeletal motion. C-C torsion modes are calculated at 260 cm^{-1},194 cm^{-1},107 cm^{-1} and 98 cm^{-1}. These modes show peaks at 261 cm^{-1},194 cm^{-1},108 cm^{-1} and 99 cm^{-1} respectively in I.R spectra. Comparison of the modes for PDMO modification II and modification III is shown in Table 4. It is seen that wag, twist, rock, and C-C stretches for CH_3 and CH_2 group modes in these two forms and skeletal deformation modes have large differences. These modes involve large coupling and are mixed with each other. The difference in the observed frequencies arises mainly because of the placement of the side group in different lateral position, which in turn brings about the change in interaction constants, which are responsible for the frequency shifts.

VIII. Characteristic features of dispersion curves

The vibrational frequencies versus phase angle curves are plotted in Fig. 2(a) & 3(a). These dispersion curves provide knowledge of the degree of coupling and information concerning the dependence of the frequency of a given mode upon the sequence length of an ordered conformation. They are also useful in calculating the density of phonon states, which in turn can be used for obtaining thermodynamic properties, such as specific heat, entropy, enthalpy and free energy. It has been observed that the intra molecular interactions (covalent, nonbonded) are generally stronger than the intermolecular interactions (hydrogen bonding and nonbonded). Crystal field only leads to splitting near the zone centre and zone boundary. The basic profile of the dispersion curves remains more or less unaltered. Thus the study of phonon dispersion in polymeric system is an important study.

CH_2 rocking and C-O stretching appear at 1006 cm^{-1} and 1017 cm^{-1} at zone center and disperses to 987 cm^{-1} and 1016 cm^{-1} at zone boundary respectively. C-O stretching slope decreases gradually moving towards zone boundary till δ=0.55 and increases with further increase in value of delta till δ=1. A sharp slope is seen in the dispersion curve of CH_2 rocking mode from δ=0.35 to δ=0.55. This mode consist of 18% contribution of CH_3 in plane bending at δ=0, which increases to 25% at δ=1. This may be responsible for the slope in the dispersion curve. Dispersion curve for mixed mode of t (CH_3) + v (C-C) shows sharp rise at δ=0.35 till δ=0.75 and becomes almost constant with gradual increase in delta value towards zone boundary. C-O asymmetric stretching appears at 945 cm^{-1} at zone center and disperses by 10 wave numbers at zone boundary. Since there is no mirror symmetry along the axis of the PDMO; no crossing appears in the dispersion curves. A slight repulsion is seen between the pair of modes at 904 $cm^{-1}$and 912 cm^{-1} when they come close to each other and exchange character to get repelled. This repulsion is seen at δ= 0.30 at which the higher one is repelled upwards and the lower one undergoes dispersion downwards. Mode at 822 cm^{-1}at zone center disperses by 28 wave vectors and appears at 787 cm^{-1}at zone boundary. This dispersion curve initially has main contribution from the main chain modes. However, as phase factor advances the side chain contribution start appearing and their contribution to dispersion curve appears in the form of both intensity and shift in position. Skeletal mode present at 507 cm^{-1} at the zone center decreases gradually till δ=0.3 and then shows sharp rise with increasing value of delta till zone boundary. Mode at 385 cm^{-1}at zone center is also a skeletal mode, which shows a sharp peak in the dispersion curve at δ=0.6 and finally appears at 280 cm^{-1} at zone boundary. Torsion present at 260 cm^{-1} at zone center shows gradual increase in dispersion curve as we move towards zone boundary. This mode disperses

by 18 wave vectors. Dispersion of 38 wave vectors is present in the skeletal mode present at 232 cm^{-1} at zone center and at 194 cm^{-1} at zone boundary. The lower two dispersion curves correspond to the four acoustic modes: two at $\delta=0$ (zone center) due to translation and rotation along the chain axis, and the other two at $\delta=\pi$ (zone boundary) due to transverse acoustic modes.

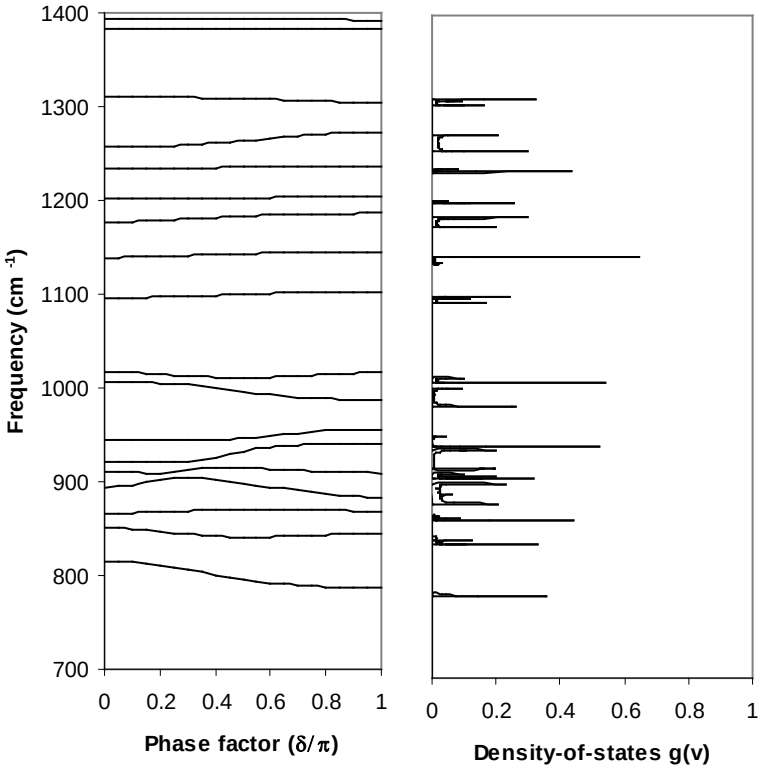

Figure 2: Dispersion curves (a) and density of states (b) of PDMO (700-1400 cm^{-1})

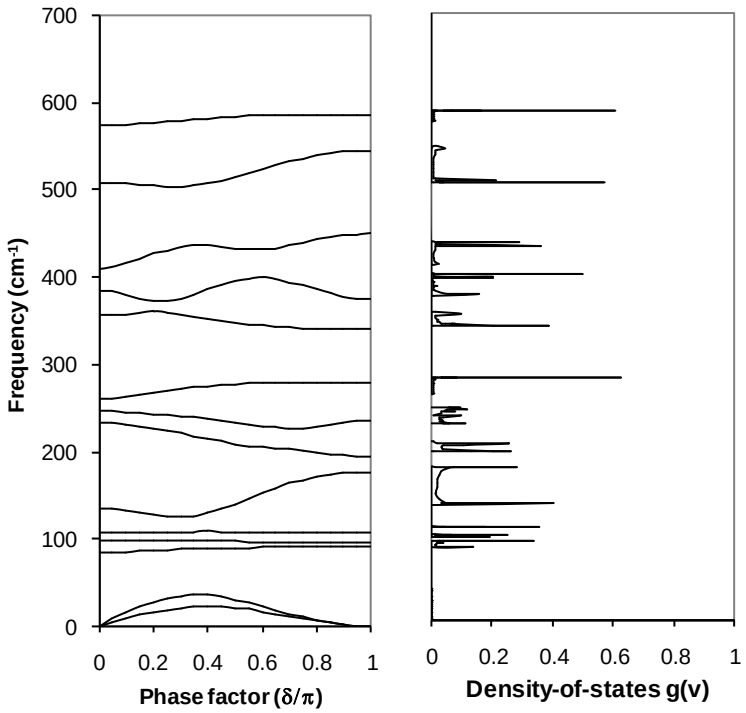

Figure 3: Dispersion curves (a) and density of states (b) of PDMO (0 -700cm^{-1})

forms shows that they are not same general profile. In form II two acoustic modes are at δ=0 (zone center) due to translation and rotation along the chain axis and other two at δ=0.57 π (zone boundary) due to transverse acoustic mode. In form III, two acoustic modes are at δ=0 (zone center) and two at□= π(zone boundary). One of the characteristic feature of the dispersion curve of PDMO is their tendency to come close and then to repel at particular delta value especially in the low frequency region. An inspection of PED at various delta values shows that in the pair of modes calculated at (261,227) and (119,113) and (108,76) repulsion takes place at □= 0.40 π, 0.45 π and 0.40 π respectively. Beyond these delta values the respective modes exchange their characters and diverge. This indicates coupling between various modes at that particular phase value. No such feature is seen in form III at lower frequencies; rather this repulsive nature of dispersion curves is present at higher frequency range (900-925) cm^{-1}. No crossing point is seen in the dispersion profile of two polymorphic forms of PDMO, due to absence of mirror symmetry.

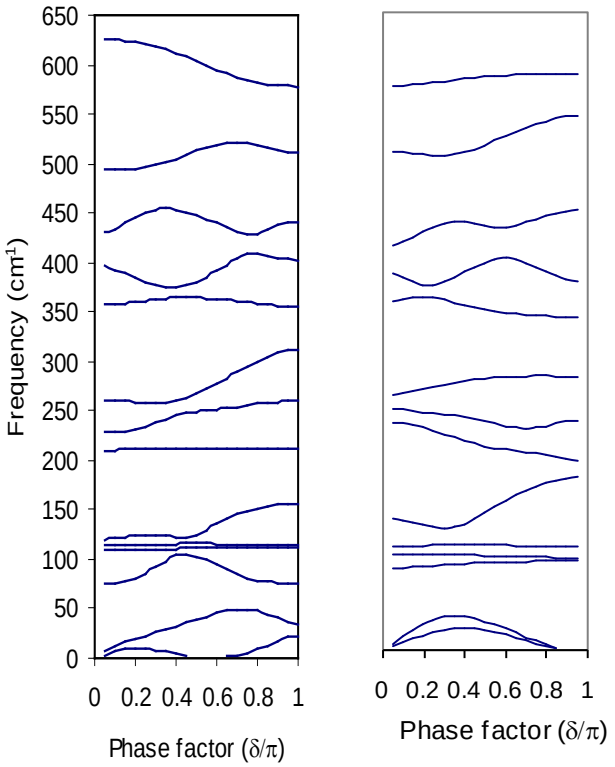

Figure 4: (a) Dispersion curves of PDMO (II) (b) and dispersion curves of PDMO (III)

X. Frequency distribution function and heat capacity

A study of the dispersion curves is important to appreciate the origin of symmetry dependent and symmetry independent spectral features. It also enables the calculation of frequency distribution function. The frequency distribution function (density-of-states) shows how the energy is distributed among the various branches of the normal modes. Figs. 2(b) and 3(b) show the plots of density-of-states versus frequency as obtained from the dispersion curves. The peaks of the frequency distribution curves correspond to regions of high density-of-states (Von Hove type singularities).

The frequency distribution function can also be used to calculate the thermodynamical properties such as heat capacity, enthalpy changes, etc. It has been used to obtain the heat capacity as a function of temperature. Heat capacity of PDMO-III has been calculated in the temperature range of 10- 300 K using Debye's equation. Beyond 20 K the specific heat rises sharply and it becomes constant at higher temperature. It is typical to describe the heat capacity variation in one dimensional system which has an initial large variation but later on it slows down. It may be added that the three dimensional picture, specially the lattice modes are not considered in this work. The extension of the present calculations in the ultra low temperature region would be meaningful when the calculation are done with the three dimensional system. This problem is very difficult not only in terms of prohibitive dimensionality but also in terms of potential field. Many interactions would be even difficult to visualize. In spite of several such limitations involved in the vibrational dynamics and concomitant thermodynamic behavior of polymeric systems, the work on an isolated chain is always a useful starting point.

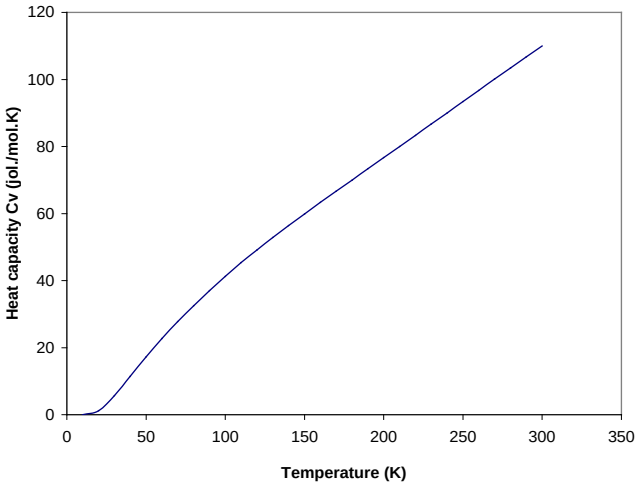

Figure 5.8 Variation of heat capacity as a function of temperatur

X. Conclusion

All characteristic features of the dispersion curves such as regions of high density of states convergence & divergence of modes near the zone center/boundary have been well interpreted from the vibrational dynamics of PDMO. In addition the heat capacity as a function of temperature in the region 10 K to 300 K has been successfully explained.

Table 5. 1 Internal coordinates and Urey Bradley force constants (md/Á)

Internal coordinates	Force constants
$\nu[C_{\alpha 1}\text{-}O]$	2.400
$\nu[C_{\alpha 2}\text{-}O]$	2.450
$\nu[C_{\alpha 1}\text{-}C]$	2.470
$\nu[C_{\alpha 2}\text{-}C]$	2.600
$\nu[C\text{-}C_{\beta}]$	2.190
$\nu[C_{\alpha 1}\text{-}H]$	4.160
$\nu[C_{\beta}\text{-}H]$	4.089
$\nu[C_{\alpha 2}\text{-}H]$	4.230
$\varphi[O\text{-}C_{\alpha 1}\text{-}C]$	.7880(.680)
$\varphi[O\text{-}C_{\alpha 1}\text{-}H]$	.4640(.300)
$\varphi[H\text{-}C_{\alpha 1}\text{–}C]$	.4440(.220)
$\varphi[H\text{-}C_{\alpha 1}\text{-}H]$	.3600(.287)
$\varphi[C_{\alpha 1}\text{-}C\text{-}C_{\beta}]$	.5800(.580)
$\varphi[C_{\alpha 1}\text{-}C\text{-}C_{\alpha 2}]$	.5700(.570)
$\varphi[C_{\beta}\text{-}C\text{-}C_{\beta}]$	.4300(.550)
$\varphi[C_{\alpha 2}\text{-}C\text{-}C_{\beta}]$	.4180(.570)
$\varphi[C\text{-}C_{\beta}\text{-}H]$	.3830(.320)
$\varphi[H\text{-}C_{\beta}\text{-}H]$	.4000(.330)
$\varphi[C\text{-}C_{\alpha 2}\text{-}O]$	.7590(.680)
$\varphi[C\text{-}C_{\alpha 2}\text{-}H]$	.3550(.200)
$\varphi[H\text{-}C_{\alpha 2}\text{-}H]$	.3970(.155)
$\varphi[O\text{-}C_{\alpha 2}\text{-}H]$	.5720(.390)
$\varphi[C_{\alpha 1}\text{-}O\text{-}C_{\alpha 2}]$	1.450(.500)
$\tau[C_{\alpha 1}\text{-}C]$	.0296
$\tau[C\text{-}C_{\alpha 2}]$	.0289
$\tau[C_{\alpha 2}\text{-}O]$	.0200
$\tau[C_{\beta}\text{-}C]$	.0024
$\tau[C\text{-}C_{\beta}]$	.0019
$\tau[O\text{-}C_{\alpha 1}]$	.0659

Table 5.2 Observed frequency are from Ref. [13]

Nondispersive modes of PDMO form - III			
Frequency (cm^{-1})			Assignment (% PED) at δ=0
Calc.	Observed		
	IR	Raman	
2968	-	2968	$\nu[C_{\beta}\text{-}H](99)$
2968	-	2968	$\nu[C_{\beta}\text{-}H](99)$
2917	-	2917	$\nu[C_{\alpha 2}\text{-}H](98)$
2917	-	2917	$\nu[C_{\alpha 1}\text{-}H](98)$
2870	-	2870	$\nu[C_{\beta}\text{-}H](99)$
2869	-	2870	$\nu[C_{\beta}\text{-}H](98)$
2869	-	2870	$\nu[C_{\beta}\text{-}H](99)$
2869	-	2870	$\nu[C_{\beta}\text{-}H](99)$
2868	-	2864	$\nu[C_{\alpha 1}\text{-}H](92)$
2867	-	2864	$\nu[C_{\alpha 2}\text{-}H](91)$
1485	1485	1485	$\varphi[H\text{-}C_{\beta}\text{-}H](93)$
1475	-	1475	$\varphi[H\text{-}C_{\alpha 2}\text{-}H](51) + \varphi[O\text{-}C_{\alpha 2}\text{-}H](40)$
1452	1453	1452	$\varphi[H\text{-}C_{\alpha 1}\text{-}H](70) + \varphi[O\text{-}C_{\alpha 1}\text{-}H](20)$
1383	1388	-	$\varphi[C\text{-}C_{\beta}\text{-}H](48) + \varphi[H\text{-}C_{\beta}\text{-}H](44)$
1304	-	1300	$\varphi[H\text{-}C_{\alpha 1}\text{-}C](25) + \varphi[O\text{-}C_{\alpha 1}\text{-}H](19) + \nu[C_{\alpha 2}\text{-}C](15)$

Table 5.3 All dispersive modes of PDMO

All dispersive modes of PDMO							
Frequency (cm^{-1})			Assignment (% PED) at δ=0.	Frequency (cm^{-1})			**Assignment (% PED) at δ=π.**
Calc.	Observed			Calc.	Observed		
	IR	Raman			IR	Raman	
1256	-	1254	φ[C-$C_{α2}$-H](20)+φ[H-$C_{α1}$-C](16)+ φ[O-$C_{α2}$-H](15)	1273	-	1254	**φ[H-$C_{α1}$-C](34)+φ[O-$C_{α1}$-H](18) + φ[C-$C_{α2}$-H](10)**
1235	1239	-	φ[O-$C_{α2}$-H](65) +φ[C-$C_{α2}$-H](20)	1237	1239	-	**φ[O-$C_{α2}$-H](75) +φ[C-$C_{α2}$-H](10)**
1177	1186	1186	φ[H-$C_{α1}$-C](30)+ φ[O-$C_{α1}$-H](18)+φ[C-$C_{β}$-H](10)	1186	1186	1186	**φ[H-$C_{α1}$-C](36)+φ[O-$C_{α1}$-H](14)+ φ[C-$C_{β}$-H](10)**
1139	1130	-	φ[C-$C_{β}$-H](30)+ φ[C-$C_{α2}$-H](17)+φ[O-$C_{α1}$-H](10)	1145	1130	-	**φ[C-$C_{β}$-H](26)+φ[C-$C_{α2}$-H](20)+ φ[O-$C_{α1}$-H](10)**
1017	1017	1017	v[$C_{α2}$-O](30)+v[$C_{α1}$-O](18)+ φ[$C_{α2}$-O-$C_{α1}$](15)	1016	1017	1017	**v[$C_{α1}$-O](25)+φ[H-$C_{α1}$-C](15)+ φ[C-$C_{β}$-H](20)**
1006	-	1006	φ[H-$C_{α1}$-C](27)+ φ[O-$C_{α1}$-H](18)+φ[C-$C_{β}$-H](15)	987	-	1006	**v[$C_{α1}$-O](30)+ φ[H-$C_{α1}$-C](25)+ φ[O-$C_{α1}$-H](14)**
944	948	914	φ[C-$C_{β}$-H](51)+ v[$C_{α2}$-O](35)	956	948	914	**v[$C_{α2}$-O](50)+φ[C-$C_{β}$-H](32)**
920	909	-	φ[C-$C_{β}$-H](60)+ φ[C-$C_{α2}$-H](18)+v[C-$C_{β}$](10)	940	909	-	**φ[C-$C_{β}$-H](60)+v[C-$C_{β}$](20)+ v[$C_{α1}$-O](10)**
910	909	-	φ[C-$C_{β}$-H](57)+ φ[C-$C_{α2}$-H](18)+v[C-$C_{β}$](14)	909	909	-	**φ[C-$C_{β}$-H](55)+φ[C-$C_{α2}$-H](16)+ v[$C_{α1}$-O](14)**
867	873	-	v[$C_{α1}$-C](30)+ φ[C-$C_{β}$-H](29)+ v[C-$C_{β}$](14)	868	873	-	**φ[C-$C_{β}$-H](35)+v[$C_{α1}$-C](24)+ v[C-$C_{β}$](20)**
815	-	822	v[C-$C_{β}$](50)+φ[C-$C_{β}$-H](10)+ v[$C_{α1}$-O](10)	787	-	822	**v[C-$C_{β}$](50)+φ[C-$C_{β}$-H](10)+ φ[O-$C_{α2}$-H](10)**
574	575	-	φ[C-$C_{α2}$-O](27)+ φ[O-$C_{α1}$-C](21)+v[C-$C_{β}$](20)	586	575	-	**φ[C-$C_{α2}$-O](27)+ φ[O-$C_{α1}$-C](21)+ φ[$C_{α1}$-C-$C_{α2}$](10)**
507	-	490	φ[$C_{α1}$-C-$C_{α2}$](10)+ φ[$C_{β}$-C-$C_{β}$](13)+v[C-$C_{β}$](50)	545	-	490	**φ[$C_{α1}$-C-$C_{α2}$](10)+ φ[$C_{β}$-C-$C_{β}$](13)+φ[$C_{α2}$-C-$C_{β}$](24)**
385	385	-	φ[$C_{α2}$-C-$C_{β}$](30)+ φ[$C_{β}$-C-$C_{β}$](17)+t[C-$C_{α2}$](12)	375	385	-	**φ[$C_{α2}$-C-$C_{β}$](35)+φ[$C_{β}$-C-$C_{β}$](15)+ t[$C_{α2}$-O](20)**
355	354	348	φ[$C_{α1}$-C-$C_{β}$](40)+φ[$C_{α2}$-C-$C_{β}$](30)	340	354	348	**φ[$C_{β}$-C-$C_{β}$](17)+ φ[$C_{α1}$-C-$C_{β}$](40)+φ[$C_{α2}$-C-$C_{β}$](30)**
261	261	-	t[$C_{α1}$-C](33)+t[C-$C_{α2}$](25)+ t[$C_{α2}$-O](16)	279	261	-	**t[$C_{α2}$-O](35)+t[C-$C_{α2}$](25)+ φ[H-$C_{α1}$-C](10)**
232	194	-	φ[$C_{α2}$-C-$C_{β}$](37)+φ[$C_{α1}$-C-$C_{β}$](18)+ φ[O-$C_{α1}$-C](17)+φ[C-$C_{α2}$-O](15)	194	194	-	**t[$C_{α2}$-O](27)+t[$C_{α1}$-C](25)+ φ[$C_{α1}$-C-$C_{β}$](15)+φ[$C_{α2}$-C-$C_{β}$](13)**
107	108	-	t[$C_{β}$-C](90)	106	108	-	**t[$C_{β}$-C](99)**
98	-	99	t[C-$C_{β}$](95)	95	-	99	**t[C-$C_{β}$](98)**
85	-	-	**t[$C_{α2}$-O](18) + t[C-$C_{α2}$](14)+ t[C-$C_{β}$](95)**	**92**	-	-	**t[C-$C_{α2}$](64)+ t[$C_{α1}$-C](30)**

Note: Only dominant potential energy distributions are given. Observed frequencies of IR and Raman are taken from Ref [20] and Ref [22], respectively

Table 5. 4 Comparison of PDMO modification II and PDMO modification III

Assignments	Observed Frequency(cm^{-1})			
	PDMO modification II		PDMO modification III	
	IR*	Raman§	IR*	Raman§
CH_3 asymmetric stretch	2968	-	2968	-
CH_3 symmetric stretch	2870	-	2870	-
CH_2 asymmetric stretch	2917	-	2917	-
CH_2 symmetric stretch	2860	-	2864	-
CH_3 asymmetric deformation	1480	1484	1473	1475
CH_2 scissoring	1468,1460	1460	1453	1452
CH_3 symmetric deformation	1420,1388	1423	1420,1388	1420
CH_2 wag	1370,1360	-	-	1300
CH_2 twist	1275,1239	1275,1238	1353,1239	1254
CH_3 twist	1060	1059	1055	1067
CH_3 wag	1190,1110	1193,1110	1186,1017	1186
CH_2 rock	947	946	1006	972
CH_3 rock	988	980	-	1002
C-O asymmetric stretch	1003	1003	1017	1017
C-O symmetric stretch	910	912	948	914
C-O-C bending	947	946	-	1006
C-C_β stretch	-	804	-	822

References Références Referencias

1) Saxena V, Pathak A, Tandon P, Gupta VD, Singh M, Polymer 2006, 47, 5117-5123.
2) Pathak A, Saxena V, Tandon P, Gupta VD, Singh M, Polymer 2006, 47, 5154-5160
3) Agrawal R, Misra RM, Tandon P, Gupta VD. Polymer 2004, 45, 5307.
4) Misra NK, Kapoor D, Tandon P, Gupta VD. Polymer 2000, 41, 2095.
5) Takahashi Y, Osaki Y and Tadokaro H. J. Polym. Sci., Polym. Phys. Edn. 1980, 18, 1863-1878.
6) Merino JC, Pastor JM, De Saja JA, Parez E, Bello A and Fatou JG. Eur. Polym. J 1985, 21, 449.
7) Parez E, Fatou JG, Bello A, Merino JC, Pastor JM and De Saja JA. Makromol. Chem. 1985, 21, 449.
8) Gomez MA, Fatou JG and Bello A. Eur. Polym. J 1986, 22, 43.
9) Parez E, Gomez MA, Fatou JG and Bello A. Colloid. Polym. Sci. 1983, 261, 187.
10) Pastor JM, Merino JC, Gomez MA, and Bello A. J. Mol. Struct. 1986, 143, 187.
11) Merino JC, Pastor JM, De Saja JA and Christen D. J. Mol. Struct.1986, 143, 183.
12) Guo YM, Zou YF, Pan CY. Macromolecular Chem.and Phy. 2001, vol. 202, 7, 1094.
13) Merino JC, Pastor JM, De Saja JA and Christen D. Polymer 1988, 29, 661.
14) Wilson EB, Decius JC, Cross PC. Moleculer Vibrations: The theory of infrared and
15) Raman viration spactra. Newyork: Dover publications; 1980
16) Higgs PW. Proc Roy Soc (London) 1953, A220, 472.
17) Urey HC, Bradley HC. Phys Rev 1931, 38, 1969
18) Qian W, Mirikin NG, Krimm S. Chem Phys Lett 1999, 315, 125.
19) King WT, Mills IM, Crawford BL. J Chem Phys 1957, 27, 455.

This page is intentionally left blank